Green synthesis of Cu-doped ZnO nanocomposites using Phytolacca dodecandra root extract to improve photocatalytic and antibacterial activity and extend avocado shelf-life

Natsanet Woldesenbet Rayya
Jimma University
Kebena Tekle Etefa
Jimma University
Ahmed Awol Yimer
Jimma University
Guta Gonfa Muleta
Jimma University
Tamene Tadesse Beyene
tamene.tadesse@ju.edu.et

Jimma University

Article

Keywords: Phytolacca dodecandra root extract, Cu-ZnO NCs, Antibacterial activity, Photocatalytic degradation, shelf-life, green synthesis

Posted Date: October 7th, 2025

DOI: https://doi.org/10.21203/rs.3.rs-7411529/v1

Additional Declarations: No competing interests reported.

Version of Record: A version of this preprint was published at Scientific Reports on December 10th, 2025. See the published version at https://doi.org/10.1038/s41598-025-31793-6.

Green synthesis of Cu-doped ZnO nanocomposites using *Phytolacca dodecandra* root extract to improve photocatalytic and antibacterial activity and extend avocado shelf-life.

Natsanet Woldesenbet Rayya, Kebena Tekle Etefa, Ahmed Awol Yimer, Guta Gonfa Muleta*, Tamene Tadesse Beyene*

Department of Chemistry, College of Natural Sciences, Jimma University, P.O.Box 378, Jimma, Ethiopia

*** Corresponding Authors**

Beyene, T.T,*(E-Mail: tamene.tadesse@ju.edu.et,)*

Abstract: Water pollution from industrial dyes and fruit spoilage due to microbes are significant global challenges. Solutions like photocatalytic degradation and preservation techniques are essential. Coating fruits with nanomaterials can reduce microbial contamination and extend shelf life, while these materials also provide alternatives against antibiotic-resistant bacteria. The primary objective of this study was to synthesize zinc oxide (ZnO) nanoparticles (NPs) and copper-doped ZnO (Cu-ZnO) nanocomposites (NCs) using *Phytolacca dodecandra* root extract as a natural reducing and stabilizing agent, enabling multiple applications such as photocatalysis, antibacterial activity, and preservation. The synthesis employed a green, coprecipitation method, optimizing parameters like precursor salts and deionized water as the solvent. The synthesized nanomaterials were thoroughly characterized through techniques including UV–Vis spectroscopy, X-ray diffraction (XRD), Fourier-transform infrared spectroscopy (FTIR), and scanning electron microscopy (SEM). UV-Vis analysis revealed energy band gaps of 3.21 eV for ZnO NPs and 2.76 eV for Cu-ZnO NCs, indicating enhanced photocatalytic potential upon copper doping. Photocatalytic tests demonstrated degradation efficiencies of 85.2% for ZnO NPs and 98.2% for Cu-ZnO NCs, with the latter also showing stable activity over time. Furthermore, antibacterial assessments against three common pathogens showed that Cu-ZnO NCs exhibited stronger antimicrobial activity than undoped ZnO NPs. Overall, this study provides novel insights into the high-performance capabilities of Cu-ZnO nanocomposites in photocatalysis, antibacterial applications, and shelf-life extension; achieved through minimal copper doping of ZnO nanoparticles.

Keywords: *Phytolacca dodecandra* root extract, Cu-ZnO NCs, Antibacterial activity, Photocatalytic degradation, shelf-life, green synthesis

1. INTRODUCTION

The rapid increase in global population and industrialization has led to significant environmental pollution, including water contamination from organic pollutants released by industries such as textile, pharmaceutical, cosmetic, and food processing sectors[1]. Dyes like methylene blue (MB) and phenols are commonly discharged during industrial processes, with up to 20% of these dyes entering water systems [2]. These pollutants pose serious threats to ecosystems and human health due to their toxic, stable, and bioaccumulative properties. Addressing water contamination requires sustainable methods that effectively remove pollutants without causing secondary environmental impacts [3].

Certain water contaminants are frequently difficult to remove using traditional water treatment methods such coagulation, flocculation, filtration, and disinfection. On the other hand, because of their special qualities; like high surface area, tunable band gaps, and increased reactivity; nanostructured materials present viable substitutes. Recent years have seen significant advancements in the treatment of organic pollutant pollution of water due to innovative techniques such as advanced oxidation processes (AOPs), bioremediation, and nanotechnology. Nanostructured materials can efficiently absorb and degrade hazardous dyes, whereas bioremediation breaks down toxins using microbes and plants. Challenges such as uncertainties regarding the long-term ecological impacts of emerging technologies, the economic feasibility of large-scale deployment, the scalability of these solutions for industrial applications, and the lack of standardized regulatory frameworks remain to be addressed. Nonetheless, these features render them especially suitable for advanced applications like photocatalytic pollutant degradation and antibacterial therapies, which have the potential to improve water purification processes [4]. Zinc oxide nanoparticles (ZnO-NPs) are widely studied for therapeutic and diagnostic uses due to their low toxicity, biodegradability, and affordability. They are safely employed in medicine, food preservation, photocatalysis, and antimicrobial applications, effectively diffusing into food, killing microbes, and helping prevent illness [5]. However, the wide band gap of ZnO (~3.37 eV), its high excitation binding energy of 60 meV, and tendencies to agglomerate limit its potential for various applications. Doping ZnO with metals such as Cu addresses these limitations by decreasing electron recombination, lowering energy bandgaps and boosting photocatalytic performance. In Cu-ZnO nanocomposites, the photogenerated electrons preferentially gather on the Cu atoms, while the holes stay on the ZnO surface. This separation of charge carriers helps to improve the overall catalytic activity of the material [6].

Fruit spoilage caused by microbial activity is a major concern, as bacteria, fungi, and yeasts quickly break down produce, resulting in nutrient loss and diminished quality. The situation is worsened by the presence of human pathogens, which pose serious health risks and can lead to foodborne illnesses. To address this issue, proper storage, careful handling, and good hygiene practices; such as thorough washing and refrigeration; are crucial. Furthermore, applying coatings of metal oxide nanoparticles (MONPs) to fruits can help reduce microbial contamination, preserve fruit quality, and extend shelf life. Cu-ZnO nanocomposites, in particular, have demonstrated strong antibacterial properties and the ability to prolong freshness, making them versatile and sustainable solutions for improving food preservation [7]. The utilization of plant extracts as natural reducing and stabilizing agents in nanoparticle synthesis has attracted increasing interest due to their abundance of phytochemicals that promote nanoparticle formation. Green synthesis methods are advantageous because they are economical and support sustainable development goals. Recent research has employed various plant extracts, such as *Clerodendrum infortunatum*, to synthesize nanoparticles in an eco-friendly manner [6], *Melissa officinalis*[7], and *Ginkgo biloba* for ZnO NPs or Cu-ZnO NCs synthesis [9]. To the best of our knowledge, there are no existing studies that have reported the use of *Phytolacca dodecandra* root extract for the synthesis of Cu-ZnO nanocomposites (NCs) aimed at applications such as dye degradation, antibacterial activity, and shelf-life extension.

This study synthesized ZnO nanoparticles (NPs) and Cu–ZnO nanocomposites (NCs) using *Phytolacca dodecandra* extract as a natural capping and reducing agent via a coprecipitation method. The nanomaterials were characterized using UV–Vis spectroscopy, XRD, FTIR, and SEM. Silver incorporation improved the optical properties of ZnO NPs, shifting the absorption edge from 372 nm to 356 nm and reducing the bandgap energy from 3.21 eV to 2.76 eV. The functional performance was assessed through photocatalytic degradation of methylene blue (MB), antibacterial activity against *Salmonella typhi (S. typhi)*, *Escherichia coli (E. coli)*, and *Staphylococcus aureus (S. aureus)*, and avocado shelf-life extension. Copper doping enhanced photocatalytic efficiency, increasing MB degradation from 85.20% to 98.20%, and effectively prolonged avocado shelf life by minimizing color change, weight loss, moisture loss, pH variations, and titratable acidity. This work highlights *Phytolacca dodecandra* extract as an eco-friendly and sustainable route for synthesizing multifunctional ZnO and Cu–ZnO nanomaterials with applications in environmental remediation and biomedicine.

2. Materials and method

The effects of adding copper to zinc oxide were investigated by synthesizing pure ZnO NPs using the coprecipitation method. Because of its benefits, which include control over compositions, simple processing, and repeatability, the coprecipitation approach is recommended. Following mixing prepared ZnO NPs with an appropriate quantity of Cu $(NO_3)_2.3H_2O$, the resulting precipitate of Cu-ZnO NCs was calcined to produce the Cu-ZnO NCs.

2.1 Chemicals and Instruments

The chemicals used in this study included zinc nitrate hexahydrate ($Zn(NO_3)_2.6H_2O$; Alfa Aesar, India), copper nitrate trihydrate ($Cu(NO_3)_2.3H_2O$; Alfa Aesar, India), sodium hydroxide (NaOH) ≥ 99% Blulux Laboratories Ltd-121,005), MB (≥99%; Sigma-Aldrich), ferric chloride ($FeCl_3$; anhydrous), dimethyl sulfoxide (DMSO) (≥ 99.99%, Xilong Scientific Co., Ltd), hydrochloric acid Hydrochloric acid (HCl; 37%, Labserv Pronalys, Australia),deionized water (DIW), and ethanol (C_2H_5OH; Shree Renuk Sugars Ltd.India).A variety of laboratory equipment was utilized, including an oven, mortar and pestle, digital balance, hot plate, magnetic stirrer, centrifuge, filter paper, test tubes, graduated cylinders, refrigerator, Erlenmeyer flasks, cuvettes, aluminum foil, pipettes, culture plates, a ruler, and sterile forceps. Characterization was performed using the following instruments: UV-Vis Spectrophotometer (Analytic Jena, made in Germany Aspect-1.2.3.6173), FT-IR Spectroscopy (65 FT-IR Perkin Elmer), X-ray Diffraction (XRD) (X-ray diffraction, DR AWELL XRD Machine), and Scanning Electron Microscopy (SEM) (JSM-IT210, Scanning Electron Microscope).

2.2 Sample collection, preparation and extraction

We confirm that permission to collect roots of Phytolacca dodecandra was obtained from the Jimma Zone Natural Resource Management authorities. The roots were collected from Merewa Kebele in Kersa Woreda, Jimma Zone (coordinates: 7.6753° N, 36.8373° E), approximately 334 kilometers from Addis Ababa. The species was identified and officially named by botanists from the Biology Department at Jimma University, specifically Dr. Shelema Guzo, in consultation with specialists from the National Herbarium (ETH) at Addis Ababa University. A voucher specimen has been deposited in the National Herbarium under the identification number ETH 0718/23. Details regarding the specimen and the responsible identifier are provided to ensure transparency. The collection and preparation procedures adhered to

established protocols, with only minor modifications. Additionally, avocado fruits were collected from a local farm in Merewa, Jimma Town, using the same geographic coordinates.

Before preparing the plant extract, fresh *Phytolacca dodecandra* roots were collected, thoroughly washed with tap water multiple times, rinsed with deionized water, cut into small pieces, and shade-dried. The dried roots were then ground into a fine powder using a mortar and pestle and stored at room temperature.

To prepare the aqueous extract, 10 g of *Phytolacca dodecandra* powder was dispersed into 200 mL of DIW in a 500mL Erlenmeyer flask, stirred at 60 °C for 30 min, and then filtered through Whitman No. 1 filter paper. The extract was refrigerated at 4 °C for future synthesis of ZnO NPs Cu-ZnO NCs and for varies application activity [11].

2.3 Preliminary Phytochemical Screening of the Plant Extract

Phytochemical screening was conducted to identify the presence of tannins, alkaloids, saponins, and flavonoids (**Figure S1)**.

Test for Tannins: The ferric chloride test was performed by adding 3 drops of 10% ferric chloride ($FeCl_3$) to 2 mL of the extract; a dark green coloration indicated phenols' presence[12]. **Test for alkaloids**: In the hydrochloric acid test, 2 mL of the extract and 2 drops of HCl were mixed; an orange or orange-red precipitate indicated the presence of alkaloids [13].

Test for saponins: A froth test involved shaking 2 mL of the extract in water and observing stable foam formation [14].

Test for flavonoids: The sodium hydroxide test was conducted by adding 2 mL of NaOH to the extract; a yellow color indicated flavonoids [15].

2.4 **Synthesis of ZnO NPs**

ZnO NPs were synthesized using the *Phytolacca dodecandra* root extract based on protocols from previous studies [16]. To synthesize the green-mediated ZnO nanoparticles, 3.166 g of zinc nitrate hexahydrate ($Zn(NO_3)_2.6H_2O$) was dissolved in 200 mL of distilled water and stirred continuously for 30 min. Next, 10 mL of *Phytolacca dodecandra* root extract was slowly added to this solution under vigorous stirring at 25 °C. After 30 min, a few drops of 2 M NaOH were introduced gradually while maintaining stirring to adjust the pH. The mixture was then stirred for an additional 90 mins at 60 °C. Following this, the solution was cooled to room temperature and left to age for 120 min to facilitate stabilization. The resulting white precipitate was

collected via filtration, washed multiple times with distilled water and ethanol to remove residual impurities, and finally dried in an oven at 70 °C for 60 min to obtain the ZnO nanoparticle powder.

2.5 Synthesis of Cu-ZnO NCs

The synthesis followed similar steps as above with slight modifications[16]. From the dried ZnO NPs, 2 g of ZnO NPs powder was measured and dissolved in 100 mL of distilled water with constant stirring for 30 min. In the same way, 0.17 g of Cu $(NO_3)_2.3H_2O$ was measured and dissolved in 100 mL of distilled water with constant stirring for 30 min. After that, the solution of Cu $(NO_3)_2.3H_2O$ was added to the solution of ZnO NPs, drop-wise. After 30 min, a few drops of NaOH (1M) solution were added under stirring to adjust the pH, and the solution was continuously stirred for another 90 min at 60 °C.

The resultant solution was kept at room temperature, washed with deionized water and ethanol three times in order to remove impurities, centrifuged and subsequently oven-dried at 70 °C for 60 min. The obtained powder was used for different characterization and application tests (**Figure S2).**

2.6 Characterization of the Synthesized ZnO NPs and Cu-ZnO NCs

The synthesized ZnO nanoparticles (NPs) and Cu–ZnO nanocomposites (NCs) were characterized using a range of analytical techniques to evaluate their properties. UV–Vis spectroscopy was conducted over the wavelength range of 250–800 nm, with samples appropriately diluted to maintain absorbance levels between 0.1 and 1.0. This analysis provided information on surface plasmon resonance features and the energy band gaps of the materials. FTIR spectroscopy was used to analyze the functional groups and metal-oxygen bonds in solid samples, prepared as KBr pellets. Powder X-ray diffraction (PXRD) was performed using a DR AWELL XRD 700 instrument with Cu Kα radiation, scanning from 10° to 80° in 2θ to determine the crystallinity and phase composition of the samples. For morphological analysis, scanning electron microscopy (SEM) was carried out using a JSM-IT210 microscope, allowing visualization of the nanostructures and assessment of their crystallographic features.

2.7 Application of ZnO NPs and Cu-ZnO NCs

Photocatalytic Activity Test

Photocatalytic activity was assessed following literature protocols [17]. Methylene blue (MB) dye was employed as a model pollutant to assess the photocatalytic efficiency of the

synthesized ZnO nanoparticles (NPs) and Cu–ZnO nanocomposites (NCs) under visible light illumination. In brief, 40 mg of the catalyst was added to 100 mL of an aqueous MB solution (10 mg/L) and stirred in the dark for 30 min to establish adsorption–desorption equilibrium. Subsequently, the mixture was exposed to visible light irradiation to facilitate photodegradation. During the irradiation process, 5 mL aliquots were withdrawn at 10 min intervals over a total duration of 60 min. These samples were centrifuged for 10 min to remove the catalyst particles, and the supernatant's absorbance was measured using a UV–Vis spectrophotometer.

The photo degradation efficiency was calculated using Equation 1

$$Degradation\ (\%) = \frac{Co-Ct}{Co} x100 \text{----------} 1$$

Where C_o and C_t represent the dye concentrations at irradiation time of t = 0 and t = t, respectively.

Antibacterial activity test

To study the antibacterial activity of the synthesized NPs and NCs, the following experimental procedure was carried out according to the literature[18].Antibacterial testing was conducted using cultures of *Staphylococcus aureus, Escherichia coli,* and *Salmonella typhimurium* on nutrient agar plates at 37 °C. ZnO NPs and Cu-ZnO NCs solutions at 100 mg/L concentrations were prepared, and filter paper discs were impregnated with these solutions for inhibition zone measurement post-incubation. The growth inhibition zone was measured in mm after 24 hours of incubation at 37 °C and compared with the standard drug (Gentamicin). A 1% DMSO solution was used as a negative control, and Gentamicin (10 mg/mL) was used as a positive control.

Shelf-life Activity Test

Avocado fruits were collected from the Jimma Zone Kersa Woreda Morowa Kebele from the farm depending on color, ripening and mass then thoroughly washed with distilled water to remove any impurities. Each fruit was weighed using a calibrated digital balance, and the initial weight was recorded for accuracy. Then the shelf-life of treated avocado fruits was evaluated using different treatments: control (no treatment), *Phytolacca dodecandra* extract, ZnO NPs, and Cu-ZnO NCs. Treated avocados were stored in petri dishes at room temperature, and

various parameters, including moisture content (%), weight loss (%), titratable acidity (TA %), and pH, were measured weekly.

Weight Loss (%)

Avocados were weighed weekly at seven-day intervals. The initial weight of each fruit served as a baseline control, while subsequent weights recorded during storage were used as parameters for analysis. The percentage of weight loss was then calculated based on these measurements, following the methodology of [19] . Percentage of total weight loss was calculated weekly by using Equation 2:

$$Weight\ loss(\%) = \frac{\text{Initial weight} - \text{final weight}}{\text{Initial weight}} * 100\% \text{----------2}$$

Moisture contents (%)

A 10 g sample of avocado was taken and placed in a crucible, then oven-dried at 100 °C for 3 hours. After drying, the crucible was removed and transferred to a desiccator to cool, and the weight was recorded. The percentage of total moisture loss was then calculated weekly using Equation 3:

$$Moisture\ content(\%) = \frac{\text{Initial weight} - \text{final weight}}{\text{Initial weight}} * 100\% \text{----------3}$$

Titratable Acidity (TA%)

The titratable acidity (TA%) of the avocado fruits was measured using a titration method, following a protocol from the literature with slight modifications [20]. A 10 g sample of avocado pulp was homogenized with 90 mL of distilled water, and 3 to 4 drops of phenolphthalein indicator were added. The mixture was then titrated with a 0.1 M NaOH solution. The volume of NaOH used was recorded from the burette, and the concentration of the avocado pulp was calculated using Equation 4.

$$TA(\%) = \frac{(VNaOH)(M\ NaOH \times 0.064)}{(\text{V of juice titrated})} \text{X}100\% \text{----------4}$$

Whereas (V NaOH) = volume of sodium hydroxide (M NaOH) = Concentration of sodium hydroxide (V of juice) = volume of fruits sample.

Measurement of pH

The pH of the avocado fruits was measured with a digital pH meter following standard procedures. A 20 g sample was suspended in 100 mL of distilled water, and the pH was recorded using the calibrated pH meter. Prior to measurement, the pH meter was calibrated with buffer solutions of pH 4 and pH 7. The reported pH value represents the average of multiple readings.

3. RESULTS AND DISCUSSION

This additional information contains all of the materials and techniques used in this study to produce the results. **Figure S1** in the supporting documentation shows a schematic illustration of the synthesis process. The optimization of several factors, such as temperature, time, pH, and concentration, is provided in a supporting document.

3.1 Preliminary phytochemical screening of the *Phytolacca dodecandra* plant extract

Phytochemical analysis was conducted to determine the presence of bioactive compounds in *Phytolacca dodecandra* root extract, utilizing various chemical tests. The preliminary phytochemical screening of the extract showed the existence of saponins, alkaloids, flavonoids, and tannins (**Table.1**).

Table.1 Phytochemical component of *Phytolacca dodecandra* roots extract

Phytochemical	Chemical test	Result color/precipitate	Result
Saponins	Forth (foam) test	foam formation	++
Flavonoids	Sodium hydroxide test	yellow color	+
Alkaloids	Hydrochloric acid test	orange-red precipitate	+
Tannins	Ferric chloride test	Dark green	+

The presence of phytochemicals is denoted by a (+) symbol, while their absence is indicated by a (−) symbol. In this study, the plant extract was found to contain various phytochemicals, including tannins, alkaloids, flavonoids, and saponins. To confirm the presence of these bioactive compounds in *Phytolacca dodecandra* root extract, a phytochemical screening test was performed using different chemical reagents (**see Figure S2**).

3.2 Parameters Optimization for the Synthesis of Cu-ZnO NCs

This study focuses on key parameters, including the concentration of Zn $(NO_3)_2.6H_2O$, the volume of plant extract from *Phytolacca dodecandra* **(Figure S3 a and b),** pH, temperature, reaction time **(Figure S4 a-c),** and the ratio of dopant concentration **(Figure S5 a-c**). Each parameter significantly influences the nucleation rate, particle size, and uniformity of the synthesized nanomaterials. By systematically varying these parameters, optimal conditions were established for producing Cu-ZnO NCs, which demonstrate enhanced properties suitable for various applications.

3.3 Characterization of Synthesized ZnO NPs and Cu-ZnO NCs

Using UV-Vis spectroscopy, the optical absorption properties of the synthesized ZnO nanoparticles (NPs) and Cu-ZnO nanocomposites (NCs) were examined. The absorption spectra of Phytolacca dodecandra root extract, ZnO NPs, and Cu-ZnO NCs are presented in (**Figures 1a-1c)**. The extract exhibited a characteristic absorption peak at 272 nm. The formation of ZnO NPs and Cu-ZnO NCs was confirmed by their respective absorption peaks at 356 nm and 372 nm during UV-Vis analysis. These results are consistent with recent studies, such as Reference 22, where ZnO NPs and Cu-ZnO NCs synthesized from Croton macrostachyus leaf extract showed maximum absorption peaks at 368 nm and 375 nm, respectively. Additionally, the observed spectral shift toward longer wavelengths after incorporating copper into ZnO NPs suggests a reduction in the energy band gap of the ZnO nanoparticles [22]. Additionally, after doping, the absorption peak of the nanocomposites (NCs) broadened. This broadening is attributed to interactions between smaller particles, which promote particle growth. The calculated energy band gaps for the green-synthesized ZnO nanoparticles (NPs) and Cu-ZnO nanocomposites (NCs) were 3.21 eV and 2.76 eV, respectively (see Figures 1c and 1d). Generally, the energy band gap of green-synthesized ZnO NPs decreases upon incorporation of copper into the structure. This observation aligns closely with recent literature, where the band gaps of ZnO NPs and Cu-ZnO NCs were reported to be 3.17 eV and 2.68 eV, respectively [23].

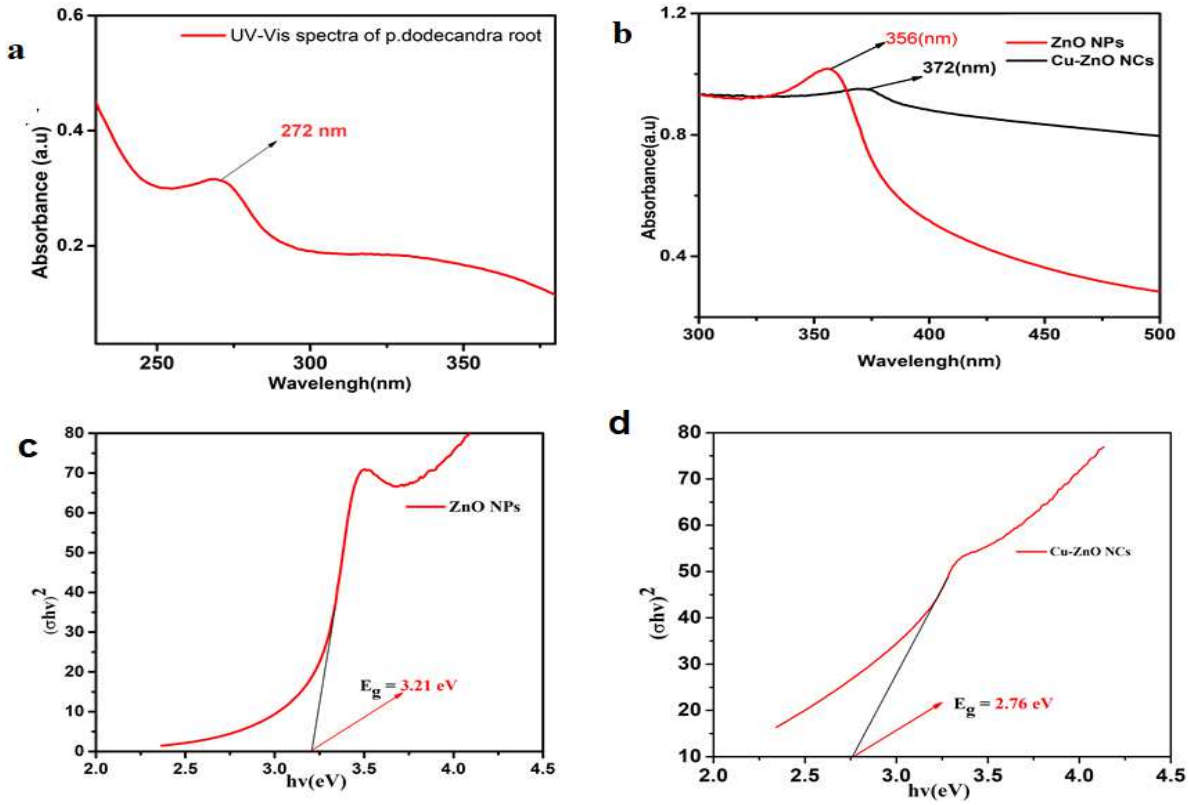

Figure 1. *UV-Vis spectra of (a) Phytolacca dodecandra root extract and (b) ZnO NPs and Cu-ZnO NCs; Tauc plots of (c) ZnO NPs and (d) Cu-ZnO NCs.*

The FT-IR spectra were utilized to identify functional groups and plant metabolites responsible for reducing and stabilizing the green-synthesized ZnO NPs and Cu-ZnO NCs. The FT-IR spectra of the synthesized ZnO NPs, Cu-ZnO NCs, and *Phytolacca dodecandra* root extract (**Figures 2a and 2b**) display a broad absorption band in the range of 3424–3467 cm^{-1}, indicating the stretching vibrations of O–H groups present in water and phenolic compounds [24]. However, after the incorporation of copper, the intensity increased, and the broad band decreased. This change may be attributed to a reduction in water content within the Cu-ZnO NCs or to interactions between copper and the hydrogen-bonded O–H groups [16]. The characteristic peaks observed between 2910 and 2929 cm^{-1} correspond to the C–H stretching vibrations of alkyl groups. These C–H and O–H functional groups are derived from flavonoids and phenolic compounds [25]. The peaks observed at 1611–1634 cm^{-1} in ZnO nanoparticles, a prominent peak at 1620 cm^{-1} in Cu-ZnO nanocomposites, and an intense peak at 1634 cm^{-1} in the *Phytolacca dodecandra* extract (**Figure 2a**) were attributed to the C=O (carbonyl) functional group. These carbonyl groups are derived from flavonoids, which serve as reducing and stabilizing agents in the synthesis of nanoparticles [26]. The prominent peak at 1385 cm^{-1} in *Phytolacca dodecandra* root extract, along with the weaker band around 1411 cm^{-1} observed

in ZnO nanoparticles, shifted to 1380 cm^{-1} after copper doping. This shift is attributed to O–H bending vibrations [27]. Vibrational modes of Zn–O were observed in the range of 400 to 700 cm^{-1}, specifically at 513 and 611 cm^{-1} for ZnO nanoparticles, and at 486 and 560 cm^{-1} following copper doping [25].

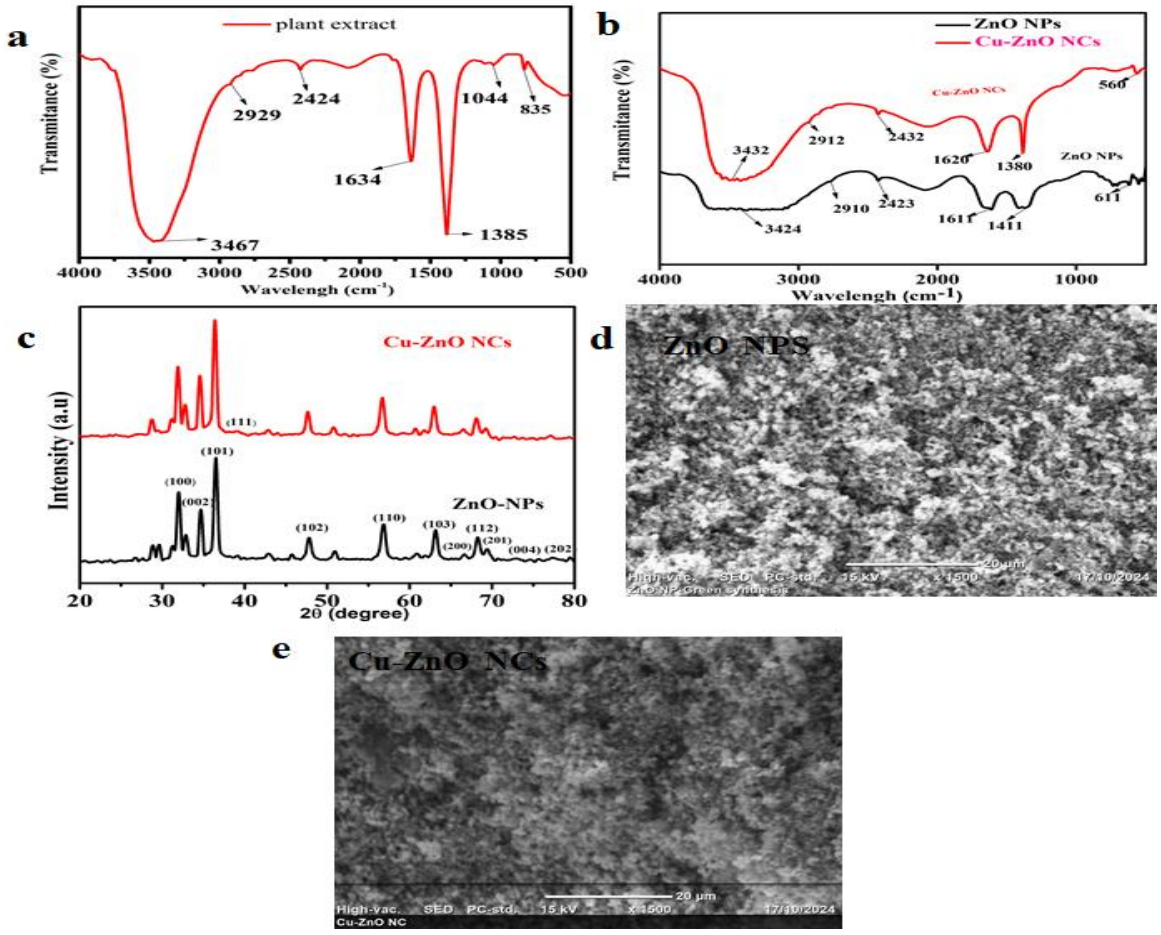

Figure 2: *(a) FTIR spectrum of the plant extract; (b) FTIR spectrum of ZnO nanoparticles; (c) FTIR spectrum of Cu-doped ZnO nanocomposites; (d) XRD patterns of ZnO nanoparticles and Cu-ZnO nanocomposites; (e) SEM image of ZnO nanoparticles; and (f) SEM image of Cu-ZnO nanocomposites***.**

For the ZnO nanoparticles and Cu-ZnO nanocomposites, prominent diffraction peaks were observed at 31.90°, 34.60°, 36.30°, 47.86°, 56.93°, 63.14°, 66.68°, 68.27°, 69.49°, 73.11°, and 77.57°, corresponding to the (100), (002), (101), (102), (110), (103), (200), (112), (201), (004), and (202) crystal planes. These peaks confirm the hexagonal structure of ZnO crystals, which are consistent with the monoclinic phase. The 2θ values align well with the reference data from JCPDS card no. 79-2205, indicating that the ZnO nanoparticles possess a crystalline

monoclinic structure [28]. The XRD analysis suggests that the incorporation of copper into the ZnO nanoparticles had little impact on the overall crystallinity of the Cu-ZnO nanocomposites.

The reduced intensity of the CuO (111) diffraction peak was attributed to the low copper content (8%) in the Cu-ZnO nanoparticles. The presence of CuO was confirmed by matching the diffraction peak at a 2θ value of 39.1°, corresponding to the (111) plane, with data from JCPDS Card No. 48-1548. (Figure 2c) [29]. The diffraction patterns of hexagonal ZnO (JCPDS card no. 01-080-0074) [30] and Cu-ZnO nanocomposites closely resemble those of pure ZnO nanoparticles, confirming their similarity. The minor additional peaks observed in the PXRD patterns may be due to trace impurities introduced during sample preparation and handling [31]. These findings align with previous studies indicating that incorporating small amounts of copper into the ZnO matrix does not significantly change the crystal structure. The average crystalline sizes of the Cu-ZnO nanocomposites and ZnO nanoparticles were estimated using the Scherrer equation, as shown in Equation 5

$$D = \frac{0.9\lambda}{\beta \mathrm{Cos}\theta} \quad \text{.....5}$$

Whereas D is the average crystallite size (in nanometers, nm) K is the Scherrer constant, which is usually taken as 0.9λ is the X-ray wavelength (in nanometers, nm), β is the full width at half maximum (FWHM) of the diffraction peak (in radians), θ is the Bragg angle (in radians). The crystalline sizes of Cu-ZnO nanocomposites and ZnO nanoparticles synthesized using Phytolacca dodecandra root extract were measured to be approximately 19 nm and 24 nm, respectively. The reduction in crystal size observed in Cu-ZnO NCs compared to pure ZnO NPs can be attributed to several factors: the incorporation of CuO dopant induces lattice distortions that hinder the growth of larger crystals; it promotes nucleation, resulting in smaller particles; limited solubility of copper may lead to segregation, preventing the formation of bigger crystals; it alters thermodynamic conditions to favor the stability of smaller particles; and the presence of defects and dislocations further impedes crystal growth [32]. This result was in close agreement with the literature [33] that reported crystalline size of Cu-ZnO NCs were 20.73 nm.

The surface morphologies of the synthesized ZnO nanoparticles and Cu-ZnO nanocomposites were examined using SEM. The SEM images of ZnO NPs and Cu-ZnO NCs are shown in (**Figures 2d and 2e)**. Based on these images, the ZnO NPs display a relatively uniform size distribution, minimal aggregation, and a spherical morphology. These observations are

consistent with recent literature reports that describe ZnO nanoparticles as predominantly spherical in shape [34].The morphology of Cu-ZnO NCs is significantly improved compared to ZnO NPs. This image shows almost spherical forms and a less agglomerated, nearly uniform appearance, but the individual features appear to be even smaller in size compared to the previous ZnO NPs samples. There is good agreement between the calculated particle size from the XRD patterns and the morphology of the synthesized materials. It is worth mentioning that dopping copper to ZnO NPs improved stability and morphology by modifying surface characteristics as revealed by the FT-IR analysis. This result was in close agreement with the literature [34].

3.4 Photocatalytic activity

The photocatalytic degradations of the methyl blue (MB) dye were studied in the present work using ZnO-NP and Cu-ZnO NCs. Then, at intervals of 10, 20, 30, 40, 50, and 60 min, the ZnO-NPs and Cu-ZnO NCs were exposed to sunlight (@ Jimma). The dye degradation process began with a gradual change in the dye solution's color from blue to colorless. This was followed by a gradual decrease in the distinctive MB absorption peak strength, which was measured at 666 nm.

3.5 **Effect of reaction parameters on photocatalysis**

Several requirements for photocatalysis were carefully adjusted before to the actual test. These included the effects of catalyst dose, time of contact, pH of the point of zero charges, and initial dye concentration.

3.5.1 Effect of initial MB Dye concentration

Dark equilibration of 30 min was performed for both ZnO NPs and Cu-ZnO NCs to allow adsorption of organic pollutants, as photocatalytic reactions primarily occur in the adsorbed phase (**Figure S6a and S6b**). At lower dye concentrations, higher degradation rates are observed due to better adsorption and more available active sites. Conversely, higher dye concentrations lead to saturation of these sites, limiting adsorption and reducing degradation efficiency. The study results indicate that photocatalytic activity is highest at 10 mg/L MB concentration, achieving a maximum of 94% degradation with Cu-ZnO NCs (**Figure 3a**), but declines at higher concentrations due to reduced photon penetration and hydroxyl radical formation.

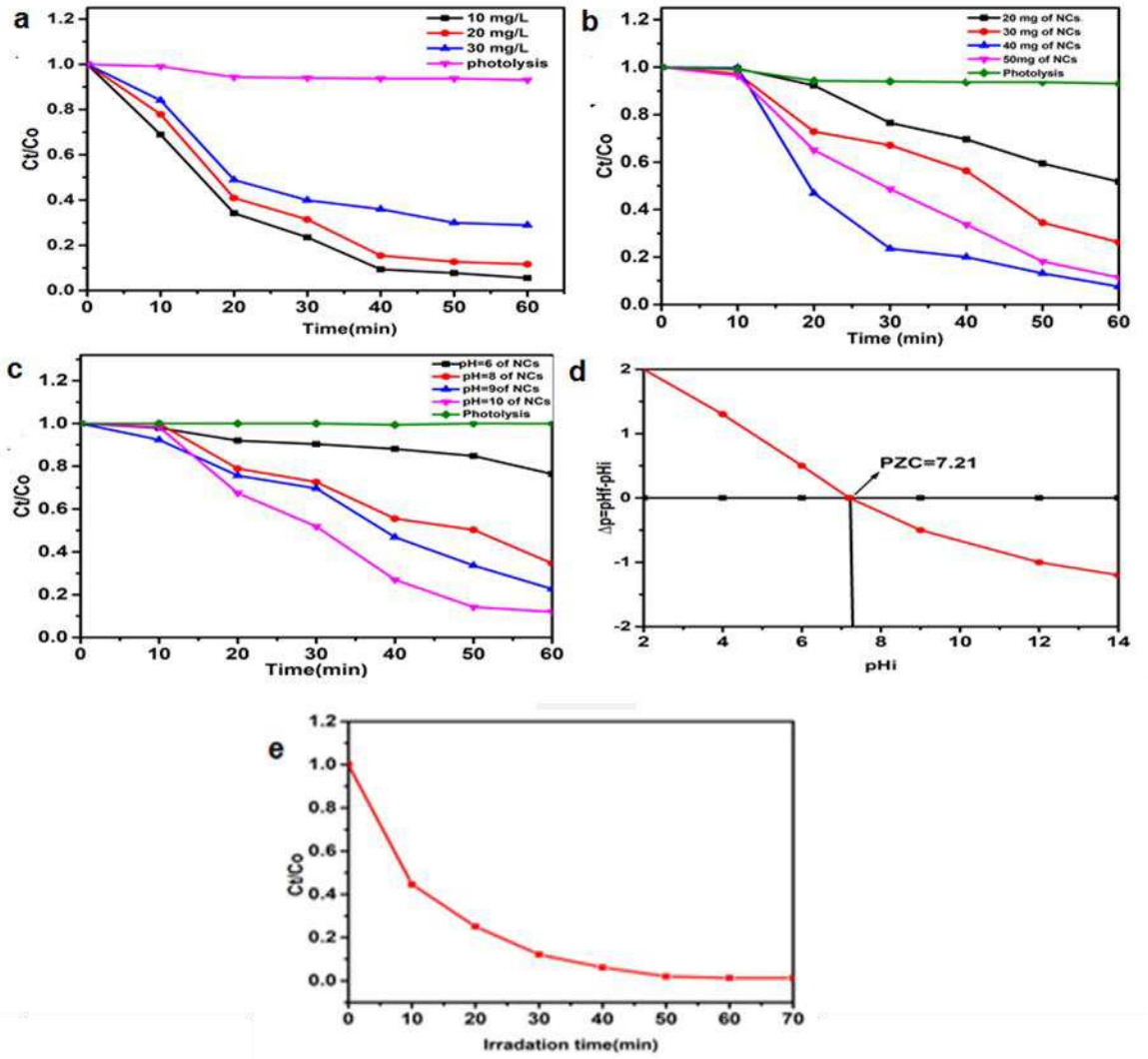

Figure 3. *Degradation efficiency of MB influenced by various parameters: (a) initial MB concentration, (b) Cu-ZnO NCs dosage, (c) solution pH, (d) point of zero charge, (e) irradiation time, and (f) reusability and stability tests.*

Effect of Catalyst Dose

From an economic perspective, the amount of photocatalyst is a key factor influencing pollutant degradation efficiency. Determining the optimal dose is essential to balance effective dye removal with resource use. As the dosage of ZnO NPs and Cu-ZnO NCs increased from 20 mg to 40 mg, MB degradation improved from 38.4% to 82.10% and 49.21% to 92.12%, respectively (**Figures 3b and S7b**). However, further increasing the catalyst dose from 40 mg to 50 mg resulted in a gradual decline in degradation efficiency, likely due to increased light reflectance and turbidity, which hinder light penetration and reduce photocatalytic activity [35].

Therefore, it was shown that the 40 mg catalyst dosage was optimum for the photocatalytic degradation of 10 ppm MB.

3.5.2. Effect of pH

This study determined the PZC of ZnO NPs and Cu-ZnO NCs within a pH range of 2–14. Above the PZC, the composites favored adsorption of positively charged particles, while below it, they preferentially adsorbed negatively charged dyes. Adjusting the solution pH can thus modulate surface charge for selective dye degradation (**Figure 4d and S7d**). The Ct/Co plots showed that MB degradation on Cu-ZnO NCs increased with pH up to 10. At pH 6, competition from H+ ions and repulsion between dye cations and positively charged sites limited removal. Beyond pH 8–10, electrostatic attraction improved, but further pH increases did not enhance degradation, indicating a plateau. Optimal MB removal (~93.8%) occurred at pH 10 under 60 min of irradiation, which is consistent with previous findings [36].

3.5.3. Effect of Contact Time

The impact of irradiation time on MB dye degradation was assessed using UV-Vis absorbance spectra, which quantified the degradation percentage to determine the optimal exposure duration for maximum efficiency. Experiments were conducted under optimal conditions: pH 10, 40 mg catalyst dose, and an initial dye concentration of 10 mg/L. Results showed that degradation increased with time from 0 to 70 min (**Figure 4e**), reaching a peak at 60 min with 98.20% removal. Beyond 60 min, changes in degradation efficiency were negligible. Therefore, 60 min was selected for subsequent experiments.

3.6 Degradation of MB using ZnO and Cu-ZnO NCs at Optimum Conditions

The photocatalytic degradation of methylene blue (MB) was studied using pure ZnO NPs and Cu-ZnO NCs. In contrast, MB without a catalyst showed minimal degradation under light, indicating that self-degradation of MB is insignificant (**Figure 5 a**). In the dark, both ZnO NPs and Cu-ZnO NCs exhibited small absorbance peaks, with Cu-ZnO NCs showing a more rapid decrease in peak intensity upon light exposure, nearly disappearing after 60 min (**Figure 5 b-5e**). This enhanced degradation efficiency of Cu-ZnO NCs compared to ZnO NPs is primarily due to the narrower band gap and superior surface properties of the Cu-doped structure, which allows better light absorption, increased electron-hole pair generation, and improved charge separation. Additionally, the presence of copper enhances surface defects, providing more active sites for MB adsorption and reducing charge carrier recombination. The slower degradation observed in ZnO NPs is attributed to their higher energy band gap, while Cu-ZnO NCs showed greater photocatalytic activity due to their modified properties (**Figure 5 f**).

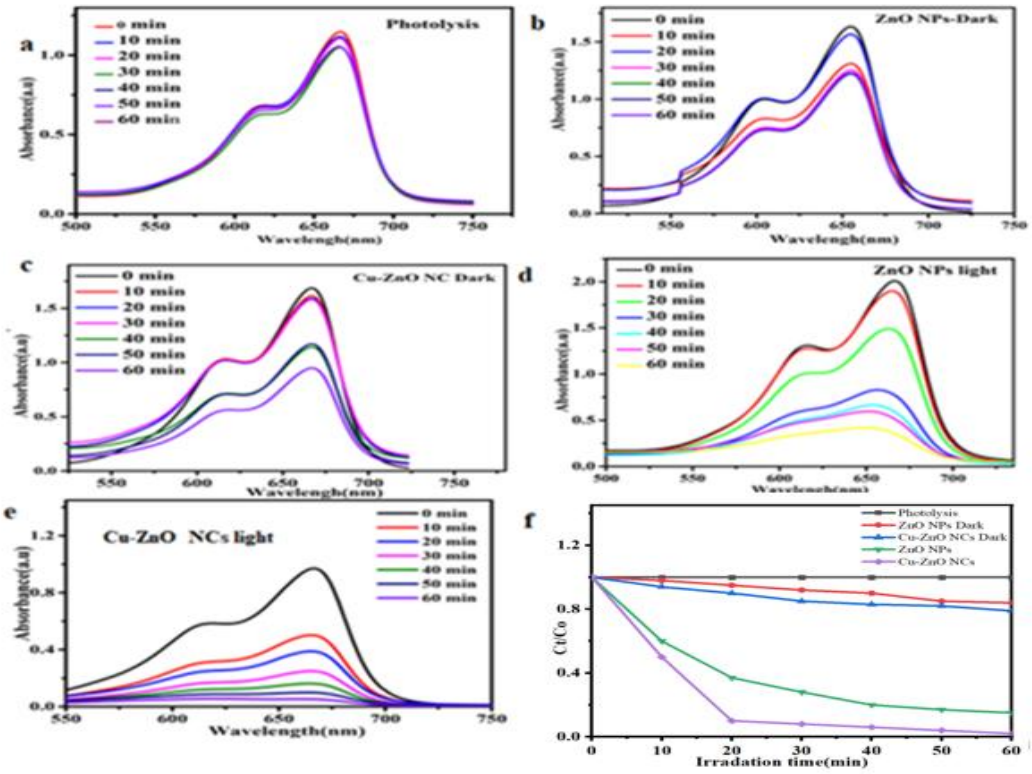

Figure 4. *Effect of irradiation time on MB degradation using: (a) ZnO NPs in dark conditions, (b) ZnO NPs under sunlight, (c) Cu-ZnO NCs in dark, and (d) Cu-ZnO NCs under sunlight. Conditions: 40 mg Cu-ZnO NCs, 10 mg/L MB dye, pH 10, with measurements at various time intervals under sunlight exposure.*

Reusability of the Photocatalytic

The reusability of catalysts in the photocatalytic degradation of MB dye was crucial for cost-effectiveness, environmental sustainability, and operational efficiency. By allowing multiple uses, these catalysts reduce overall costs and the environmental footprint associated with material production and disposal. Their ability to maintain activity over several cycles enhances the efficiency of wastewater treatment processes, making them a vital component in developing sustainable and effective methods for dye degradation[1].The reusability of prepared NCs where appraised for degradation of MB dye in the optimized reaction conditions.

The catalytic studies demonstrated that Cu-ZnO NCs maintained a high level of activity over three cycles, with a degradation efficiency of 98.20, 93.30, and 90.80% in the first, second, and third cycles, respectively (**Figure 5**). This slight decline in activity (1.80, 6.70, and 9.20% reduction per cycle) can be attributed to factors such as a decrease in catalyst dose during recovery or under-adsorption of reactants or products on the catalyst surface, which reduces its effectiveness. The gradual loss in efficiency and reusability is further explained by two main

factors: first, surface fouling from reaction intermediates, products, and contaminants reduces the available active surface area, limiting reactant adsorption and interaction, and hindering light absorption and charge carrier generation. Second, the Cu-ZnO NCs may not fully recover their initial activity between cycles due to partial deactivation of active sites, such as loss or modification of surface functional groups, defects, or heterostructure interfaces. This incomplete regeneration leads to a gradual decline in the photocatalyst's performance over successive cycles.

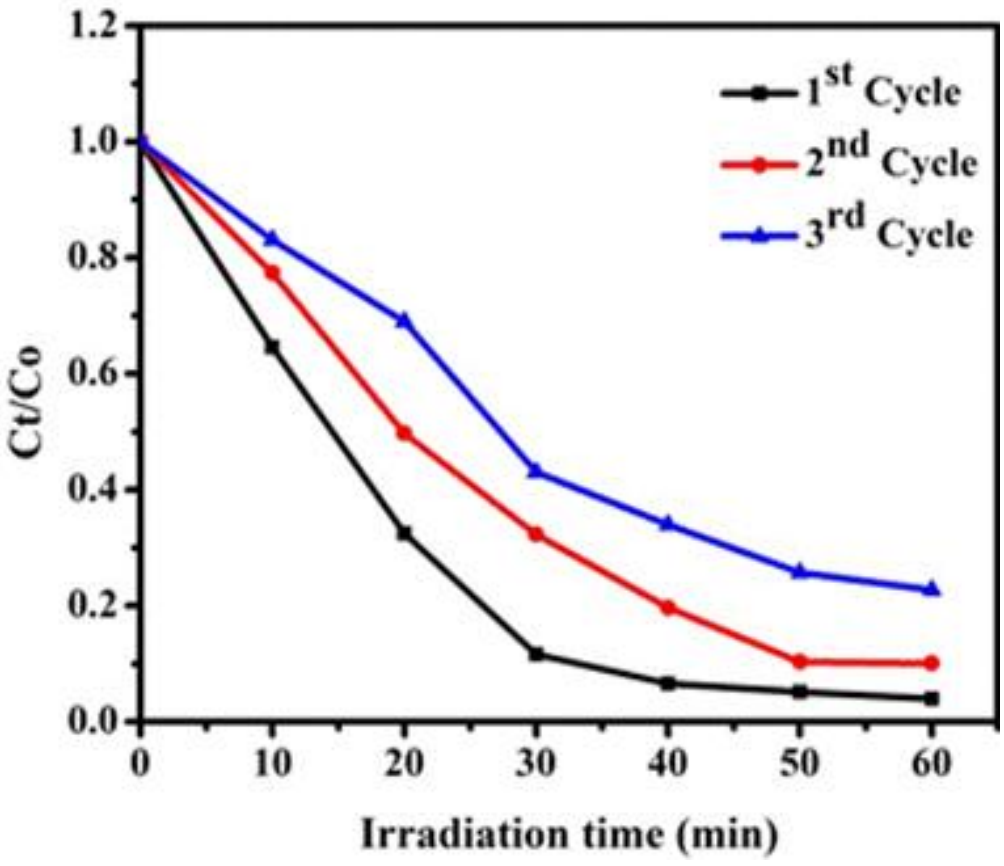

Figure 5. *Reusability of Cu-ZnO NCs evaluated under the same optimal conditions used in this study: an initial dye concentration of 10 ppm, a catalyst dose of 40 mg, pH 10, and an irradiation time of 60 min.*

Table.2 *Comparison of the Cu–ZnO NCs Photocatalyst Synthesized Using* ***Phytolacca dodecandra*** *root extract with Previously Reported ZnO-Based NCs for Photocatalytic Degradation of MB*

Synthesized NCs	% of dye degradation efficiency	Source of light	Time (min)	MB dye concentration	Catalyst Dose (mg)	Reference
CuO–ZnO	95.6	Vis	120	10^{-3} M	25	[37]
CuO–ZnO	82.00	Vis	105	20 ppm	40	[38]
CuO–ZnO	93.00	Vis	60	20 ppm	20	[39]
Cu-ZnO NCs	98.20	Sun light	60	10ppm	40	This study

Table.2 indicate that the synthesized Cu-ZnO NCs was effective for the degradation of MB dye in 60 min, based on the comparison data above, which shows that the current work was a good result with high degradation efficiency in a short time**.**

3.7.Shelf-life Analysis

3.7.1. Weight Loss of Avocado Fruits

Weight loss is a primary factor influencing the shelf life and quality of fresh fruits. In this study, it was observed that weight loss decreased as storage time (days) increased. Uncoated avocados exhibited the highest weight loss compared to those coated with various materials. Specifically, avocados coated with Phytolacca dodecandra root extract, ZnO nanoparticles, and Cu-ZnO nanocomposites showed weight losses of 21.84 ± 0.12%, 13.00 ± 0.31%, 12.90 ± 0.28%, and 4.90 ± 0.234%, respectively (**Figure 6a**). Notably, avocados coated with Cu-ZnO nanocomposites demonstrated significantly lower weight loss compared to those coated with Phytolacca dodecandra root extract or ZnO nanoparticles (**Table S1**). These results suggest that incorporating Cu-ZnO nanocomposites effectively reduces weight loss in avocado fruits, likely due to their barrier properties that limit oxygen and moisture permeability. The reduction in weight loss can also be attributed to the barrier effect of the coating material, which helps slow metabolic processes associated with postharvest deterioration. During postharvest storage, climacteric fruits undergo metabolic changes that contribute to weight loss, and these findings align with recent studies on fruit preservation [40].

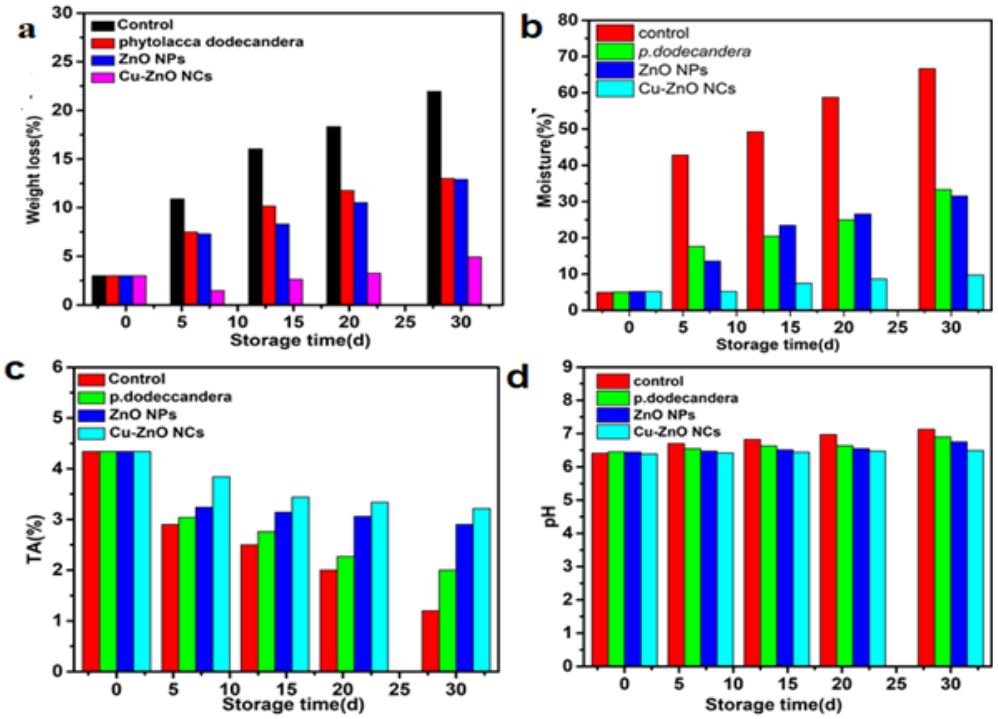

Figure.6. *Effect of avocado fruits coating on the changes in PLW of (a) weight loss %, (b) moisture loss %, (c) TA% and (d) pH.*

3.7.2. Moisture Content

The application of coatings with *Phytolacca dodecandra* root extract, ZnO nanoparticles, and Cu-ZnO nanocomposites, in conjunction with the storage period, significantly influenced the moisture content loss in avocado fruits (**Figure 6b and Table S2**). As storage time increased, moisture loss also rose markedly, reaching its peak on the 30th day for all treatments. Beyond this point, the avocados began to spoil. Importantly, all coated samples exhibited less moisture loss compared to the uncoated control fruits. Specifically, avocados coated with Cu-ZnO nanocomposites showed a moisture loss of 9.50 ± 0.17%, whereas control avocados lost 66.26 ± 0.37%. In comparison, avocados coated with *Phytolacca dodecandra* extract and ZnO nanoparticles exhibited moisture losses of 33.03 ± 0.34% and 31.37 ± 0.32%, respectively, after 30 days. The reduction in water content contributed to weight loss and fruit shrivelling during postharvest storage [20] . However, the fact that coating restricts water loss and maintains high fruit weight during storage was well documented. This was supported by [19], who also observed weight retention in mango fruits by coating ZnO NPs. The results of this study show that Cu-ZnO NCs reduced avocado fruit moisture loss as compared to control.

3.7.3. Titratable acidity (TA %)

In similar manner with the other parameters, during the storage period, the titratable acidity percentage (TA%) of avocado was significantly influenced by coatings containing *Phytolacca dodecandra*, ZnO nanoparticles, and Cu-ZnO nanocomposites. A decline in TA% was observed over time in the control, Phytolacca dodecandra, ZnO NPs, and Cu-ZnO NCs treatments as storage progressed (**Figure 6c and Table S3**). Notably, the TA% in avocados coated with Cu-ZnO nanocomposites remained higher than in the control and other treatments throughout storage. By the 30th day, TA% values across all treatments ranged from 1.22 ± 0.12% to 3.25 ± 0.12%. All coated avocado samples showed relatively higher TA% increases, indicating that the Cu-ZnO NCs treatment delayed ripening, while the ZnO NPs and Phytolacca dodecandra treatments exhibited faster ripening. Fluctuations in acidity during maturation may be attributed to the conversion of acids into sugars and their subsequent utilization in metabolic processes within the fruit. Although avocado acidity generally decreases with increasing storage time, differences among treatments were evident. After 30 days, the Cu-ZnO NCs-coated avocados maintained higher TA% values, whereas the control fruits exhibited significantly lower acidity, likely due to the absence of coating and the rapid reduction of acidity. These findings align with previous studies that reported similar trends in pH and acidity shifts in papaya fruits coated with XG (Xyloglucan) [20], supporting the conclusion that coating treatments can effectively influence postharvest fruit acidity.

3.8.4. pH of avocado fruits

In this study, the pH values of avocado samples coated with Phytolacca dodecandra extract, ZnO nanoparticles, and Cu-ZnO nanocomposites were monitored over the storage period. Initially, on day one, the pH of the avocado fruit was 6.39 ± 0.12. After seven days, the pH values changed to 7.23 ± 0.06 for the control, 6.79 ± 0.05 for the *Phytolacca dodecandra* extract, 6.66 ± 0.10 for ZnO NPs, and 6.48 ± 0.09 for Cu-ZnO NCs. After four weeks, results showed that avocados treated with Cu-ZnO nanocomposites exhibited lower pH values compared to the other treatments (**Figure 7d and Table S4**). At the end of storage, the pH of the control was 7.23 ± 0.06, while the coated samples with ZnO NPs and *Phytolacca dodecandra* extract maintained higher pH levels than the Cu-ZnO NCs-treated fruit. This suggests that the Cu-ZnO nanocomposite composition contributed to slower ripening and helped preserve acidity for a longer period. By day 30, the pH of the Cu-ZnO NCs-treated avocado was 6.48 ± 0.09, representing only a 0.09 reduction from its initial value. These

findings are similar to results observed in studies on guava fruit, where coating treatments influenced pH stability during storage [41].

3.9. Antibacterial Activity

The antibacterial efficacy of metal oxide nanoparticles (MONPs), particularly ZnO and copper-doped variants, is greatly affected by their particle size and surface characteristics. Consequently, optimizing the synthesis process and controlling the size of ZnO nanoparticles (NPs) and Cu-ZnO nanocomposites (NCs) can enhance their activity against a broader spectrum of bacterial pathogens. To assess the antibacterial properties of *Phytolacca dodecandra* root extract, as well as synthesized ZnO NPs and Cu-ZnO NCs, the disk diffusion method was employed against both Gram-positive and Gram-negative bacterial strains. Gentamicin served as the positive control, while DMSO was used as the negative control. The antibacterial activity of 100 mg/mL concentrations of the synthesized nanoparticles was evaluated against Staphylococcus aureus, Escherichia coli, and Salmonella typhi (see Figures 8a–c).

Table 3. *Effect of* ***Phytolacca dodecandra*** *extract, ZnO nanoparticles (NPs), and Cu-ZnO nanocomposites (NCs) on selected bacterial strains. Gentamicin and DMSO were used as positive and negative controls, respectively.*

Materials	***Microbial* Inhibition Zone (mm)**		
	E. Coli	***S. typhea***	***S. Aureus***
Cu-ZnO NCs	16 ± 0.20	15 ± 0.16	18 ± 0.14
ZnO NPs	12 ± 0.17	16 ± 0.18	13 ± 0.13
Plant Extract	9±0.12	10±0.11	8±0.30
DMSO	0	0	0
Gentamycin	24±0.15	23±0.20	22±0.25

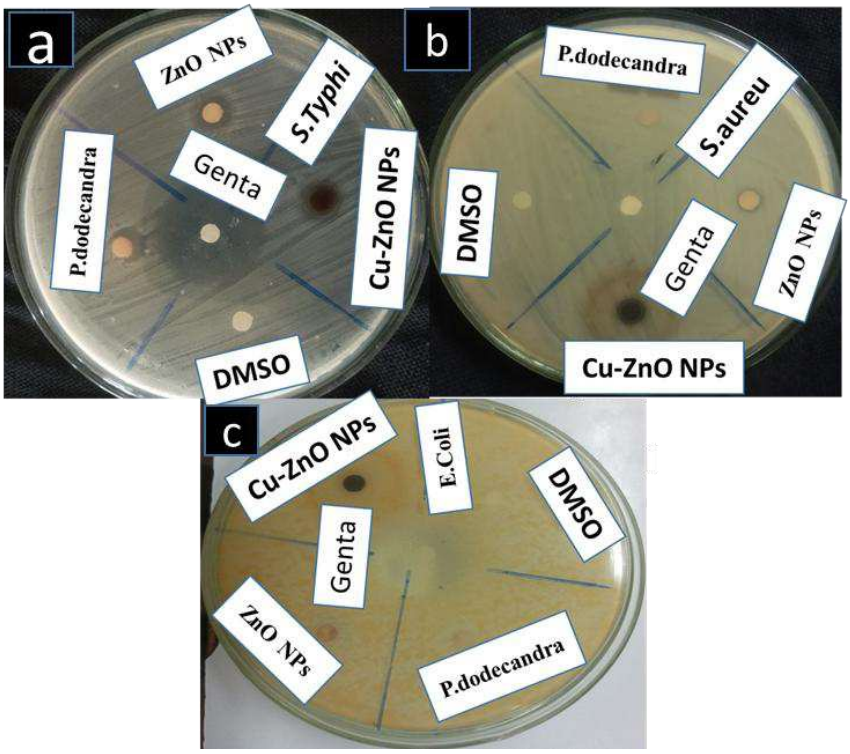

Figure 7. *Antibacterial activity of ZnO-NPs, and Cu-ZnO NCs on (a) S.aureus (b) S. Typhi and (c) E. coli*

In this study, Cu-ZnO nanocomposites (NCs) exhibited the largest zones of inhibition against all tested bacterial strains compared to ZnO nanoparticles (NPs) and Phytolacca dodecandra root extract (**Table 3**). The enhanced antibacterial activity of Cu-ZnO NCs is attributed to the strong affinity of Cu+ ions for sulfur atoms in bacterial thiol proteins. This interaction results in the cleavage of disulfide bonds within the proteins, leading to the disruption of their tertiary structure and ultimately causing bacterial cell death [42]. Antibacterial activity increases with higher concentrations of ZnO nanoparticles (NPs) and Cu-ZnO nanocomposites (NCs) (Figure S9). Since the maximum inhibitory zone was observed at a concentration of 100 mg/L, this dose was selected as the optimal amount. Cu-ZnO NCs possess a more accessible surface that can generate greater amounts of reactive oxygen species (ROS) compared to ZnO NPs. Doping zinc oxide with copper introduces additional surface defects on Cu-ZnO NCs, which further enhances ROS production. The increased presence of surface defects leads to higher ROS levels, thereby more effectively inhibiting bacterial growth. These findings align with previous research indicating that doping ZnO with metals such as silver (Ag) or copper (Cu) enhances its antibacterial activity [43].

The results of this study also showed that Gram-positive bacteria, specifically *S. aureus*, were more susceptible to the biosynthesized ZnO nanoparticles (NPs), Cu-ZnO nanocomposites (NCs), and *Phytolacca dodecandra* root extract compared to Gram-negative strains such as *E. coli* and *S. typhi. S. aureus* demonstrated greater sensitivity to both ZnO NPs and Cu-ZnO NCs. Copper and zinc ions have a higher affinity for amines and carboxyl groups, which are more abundant on the surface of cells, particularly in Gram-positive bacteria[44]. These bacteria are more susceptible to antibiotic-induced mortality due to their thick cytoplasmic membranes. Additionally, Gram-positive bacteria can absorb nanoparticles more effectively than Gram-negative bacteria because of their thick peptidoglycan-rich cell walls, which is a defining feature of Gram-positive bacteria[42]. Cu-ZnO NCs have a smaller energy band gap, with compare to ZnO NPs which indicates that as NPs get smaller, they can more easily enter bacterial cells and kill them. In contrast, gram-negative bacteria, such as *Escherichia coli*, have lipopolysaccharides that have a significant antibiotic resistance[18].The aqueous solution's *Phytolacca dodecandra* extract's antibacterial activity against particular bacterial species was also examined. The zones of inhibition for *Salmonella typhi, Escherichia coli,* and *Staphylococcus aureus* were 10±0.11, 8±0.30, and 9±0.12 mm, respectively, evaluated against this aqueous extract.

4. Conclusion

This study successfully demonstrates the eco-friendly green synthesis of ZnO nanoparticles (NPs) and Cu-ZnO nanocomposites (NCs) utilizing Phytolacca dodecandra root extract through a safe coprecipitation method that avoids hazardous chemicals. UV-Vis spectrophotometry confirmed the optical characteristics of the synthesized nanoparticles, showing absorption peaks at 356 nm for ZnO NPs and 372 nm for Cu-ZnO NCs. The band gap energy decreased from 3.21 eV in ZnO NPs to 2.76 eV in Cu-ZnO NCs, likely due to increased particle size and surface deposition of Cu^{2+} ions, which enhances resistance to electron-hole recombination. FT-IR analysis identified functional groups, especially hydroxyl groups that are essential for the reduction and stabilization of the nanoparticles, confirming successful synthesis. PXRD patterns revealed the crystalline structures of both ZnO NPs and Cu-ZnO NCs. SEM images displayed distinct morphologies, with ZnO NPs appearing spherical and Cu-ZnO NCs exhibiting a triangular shape. Photocatalytic degradation experiments optimized parameters such as catalyst dose, dye concentration, irradiation time, and pH. Under optimal conditions; 40 mg of Cu-ZnO NCs, 10 mg/L dye concentration, 60-min irradiation, and pH 10; achieved a degradation efficiency of 98.20%, significantly higher than the 85.20% observed

with ZnO NPs alone. Additionally, the synthesized Cu-ZnO NCs demonstrated promising shelf-life extension when applied to avocado fruits, reducing color change, weight loss, moisture loss, pH shifts, and titratable acidity over time. The dual functionality of Cu-ZnO NCs in photocatalytic dye degradation and food preservation highlights its potential for applications in wastewater treatment and post-harvest food storage industries.

Acknowledgements

•This work was financially supported by the College of Natural Sciences at Jimma University under the PG student project.

Conflict of Interest

•The authors declare that they have no known competing financial interests or personal relationships that could have appeared to influence the work reported in this paper.

Reference

(1) Etefa, K. T.; Rayya, N. W.; Nemera, D. J.; Muleta, G. G.; Beyene, T. T. Sustainable Preparation of Ag-ZnO Nanocomposites Using Persea Americana Peel Extract for Superior Antibacterial, Antioxidant, and Photocatalytic Efficacy. *Mater Sci Eng B* **2025**, *321* (May). https://doi.org/10.1016/j.mseb.2025.118562.

(2) Alsukaibi, A. K. D. Various Approaches for the Detoxification of Toxic Dyes in Wastewater. *Processes* **2022**, *10* (10). https://doi.org/10.3390/pr10101968.

(3) Muthukrishnan S, B. S.; Muthukumar M, S. M.; Rao MV, S. K. T. Catalytic Degradation of Organic Dyes Using Synthesized Silver Nanoparticles: A Green Approach. *J Bioremediation Biodegrad* **2015**, *06* (05). https://doi.org/10.4172/2155-6199.1000312.

(4) Muthuvinothini, A.; Stella, S. Green Synthesis of Metal Oxide Nanoparticles and Their Catalytic Activity for the Reduction of Aldehydes. *Process Biochem* **2019**, *77*, 48–56. https://doi.org/10.1016/j.procbio.2018.12.001.

(5) Haque, M. J.; Bellah, M. M.; Hassan, M. R.; Rahman, S. Synthesis of ZnO Nanoparticles by Two Different Methods & Comparison of Their Structural, Antibacterial, Photocatalytic and Optical Properties. *Nano Express* **2020**, *1* (1). https://doi.org/10.1088/2632-959X/ab7a43.

(6) Khan, S. A.; Noreen, F.; Kanwal, S.; Iqbal, A.; Hussain, G. Green Synthesis of ZnO and Cu-Doped ZnO Nanoparticles from Leaf Extracts of Abutilon Indicum, Clerodendrum Infortunatum, Clerodendrum Inerme and Investigation of Their Biological and Photocatalytic Activities. *Mater Sci Eng C* **2018**, *82*, 46–59. https://doi.org/10.1016/j.msec.2017.08.071.

(7) Bordbar, M.; Negahdar, N.; Nasrollahzadeh, M. Melissa Officinalis L. Leaf Extract Assisted Green Synthesis of CuO/ZnO Nanocomposite for the Reduction of 4-

Nitrophenol and Rhodamine B. *Sep Purif Technol* **2018**, *191* (May 2017), 295–300. https://doi.org/10.1016/j.seppur.2017.09.044.

(8) Osman, A. I.; Zhang, Y.; Farghali, M.; Rashwan, A. K.; Eltaweil, A. S.; Abd El-Monaem, E. M.; Mohamed, I. M. A.; Badr, M. M.; Ihara, I.; Rooney, D. W.; Yap, P. S. *Synthesis of Green Nanoparticles for Energy, Biomedical, Environmental, Agricultural, and Food Applications: A Review*; Springer International Publishing, 2024; Vol. 22. https://doi.org/10.1007/s10311-023-01682-3.

(9) Wang, Q.; Xu, S.; Zhong, L.; Zhao, X.; Wang, L. Effects of Zinc Oxide Nanoparticles on Growth, Development, and Flavonoid Synthesis in Ginkgo Biloba. *Int J Mol Sci* **2023**, *24* (21). https://doi.org/10.3390/ijms242115775.

(10) Vanlalveni, C.; Lallianrawna, S.; Biswas, A.; Selvaraj, M.; Changmai, B.; Rokhum, S. L. Green Synthesis of Silver Nanoparticles Using Plant Extracts and Their Antimicrobial Activities: A Review of Recent Literature. *RSC Adv* **2021**, *11* (5), 2804–2837. https://doi.org/10.1039/d0ra09941d.

(11) Sujitha, M. V.; Kannan, S. Green Synthesis of Gold Nanoparticles Using Citrus Fruits (Citrus Limon, Citrus Reticulata and Citrus Sinensis) Aqueous Extract and Its Characterization. *Spectrochim Acta - Part A Mol Biomol Spectrosc* **2013**, *102*, 15–23. https://doi.org/10.1016/j.saa.2012.09.042.

(12) Haida, S.; Bakkouche, K.; Kribii, A. R.; Kribii, A. Chemical Composition of Essential Oil, Phenolic Compounds Content, and Antioxidant Activity of Cistus Monspeliensis from Northern Morocco. *Biochem Res Int* **2021**, *2021*. https://doi.org/10.1155/2021/6669877.

(13) Yadesa, D.; Guyasa, J. N.; Beyene, T. T., Effect of Codoping Zinc Oxide Nanoparticles with Sulfur and Nitrogen on Its Energy Bandgap, Antioxidant Properties, and Antibacterial Activity. 2024, 2024 (1), 4275035, https://doi.org/10.1038/s41598-025-13151-8

(14) Das, B. K.; Al-Amin, M. M.; Russel, S. M.; Kabir, S.; Bhattacherjee, R.; Hannan, J. M. A. Phytochemical Screening and Evaluation of Analgesic Activity of Oroxylum Indicum. *Indian J Pharm Sci* **2014**, *76* (6), 571–575.

(15) Ali, S.; Khan, M. R.; Sajid, M.; Zahra, Z. Phytochemical Investigation and Antimicrobial Appraisal of Parrotiopsis Jacquemontiana (Decne) Rehder. *BMC Complement Altern Med* **2018**, *18* (1), 1–15. https://doi.org/10.1186/s12906-018-2114-z.

(16) Tegenaw, A. B.; Yimer, A. A.; Beyene, T. T. Boosting the Photocatalytic Activity of ZnO-NPs through the Incorporation of C-Dot and Preparation of Nanocomposite Materials. *Heliyon* **2023**, *9* (10), e20717. https://doi.org/10.1016/j.heliyon.2023.e20717.

(17) Nan, R.; Liu, S.; Zhai, M.; Zhu, M.; Sun, X.; Chen, Y.; Pang, Q.; Zhang, J. Facile Synthesis of Cu-Doped ZnO Nanoparticles for the Enhanced Photocatalytic Disinfection of Bacteria and Fungi. **2023**.

(18) Olani A, Guyasa JN, Nemera DJ, Efa MT, and Beyene TT. Impact of graphene oxide integration with ZnO nanoparticles on its photocatalytic, antimicrobial, and antioxidant

activities. Bull. Chem. Soc. Ethiop. 2025, 39(3), 515-534. https://dx.doi.org/10.4314/bcse.v39i3.1 .

(19) Rosman, N. F. Preserving Mango Quality: Assessing the Influence of Zinc Oxide Nanocomposite-Corn Starch Coating Concentrations on Postharvest Attributes. **2024**, 1–17.

(20) Kumar, N.; Pratibha; Upadhyay, A.; Trajkovska Petkoska, A.; Gniewosz, M.; Kieliszek, M. Extending the Shelf Life of Mango (Mangifera Indica L.) Fruits by Using Edible Coating Based on Xanthan Gum and Pomegranate Peel Extract. *J Food Meas Charact* **2023**, *17* (2), 1300–1308. https://doi.org/10.1007/s11694-022-01706-6.

(21) Guerra, F. D.; Attia, M. F.; Whitehead, D. C.; Alexis, F. Nanotechnology for Environmental Remediation : Materials and Applications. **2018**, 1–23. https://doi.org/10.3390/molecules23071760.

(22) Pardakhty, A.; Ranjbar, M.; Moshafi, M. H.; Abbasloo, S. A Systematic Study of ZnO/CuO Core/Shell Nanostructures Pegylated by Microwave Assistant Reverse Micelles (RM) Method. *J Clust Sci* **2018**, *29* (6), 1061–1068. https://doi.org/10.1007/s10876-018-1416-0.

(23) Mohammadi-aloucheh, R.; Habibi-yangjeh, A.; Bayrami, A.; Asadi, A. Enhanced Anti-Bacterial Activities of ZnO Nanoparticles and ZnO / CuO Nanocomposites Synthesized Using Vaccinium Arctostaphylos L . Fruit Extract. *Artif Cells, Nanomedicine, Biotechnol* **2018**, *46* (S1), S1200–S1209. https://doi.org/10.1080/21691401.2018.1448988.

(24) Jagadeeswari, R.; Rathika, G.; Satheesh Kumar, K. V.; Selvakumar, P. Electrochemical, Structural, Optical, and Morphological Characteristics of Cu-Loaded ZnO Nanostructures Synthesized from Bio-Waste (Maize) Using a Green Synthesis Technique. *Dig J Nanomater Biostructures* **2023**, *18* (1), 291–298. https://doi.org/10.15251/DJNB.2023.181.291.

(25) Das, A.; Wary, R. R.; Nair, R. G. Cu Modified ZnO Nanoflakes: An Efficient Visible Light-Driven Photocatalyst and a Promising Photoanode for Dye Sensitized Solar Cell (DSSC). *Solid State Sci* **2020**, *104* (March), 106290. https://doi.org/10.1016/j.solidstatesciences.2020.106290.

(26) Shi, W.; Yang, S.; Sun, H.; Wang, J.; Lin, X.; Guo, F. Carbon Dots Anchored High-Crystalline g-C 3 N 4 as a Metal-Free Composite Photocatalyst for Boosted Photocatalytic Degradation of Tetracycline under Visible Light. *J Mater Sci* **2021**, *56* (3), 2226–2240. https://doi.org/10.1007/s10853-020-05436-2.

(27) Faghihzadeh, F.; Anaya, N. M.; Schifman, L. A.; Oyanedel-Craver, V. Fourier Transform Infrared Spectroscopy to Assess Molecular-Level Changes in Microorganisms Exposed to Nanoparticles. *Nanotechnol Environ Eng* **2016**, *1* (1), 1–16. https://doi.org/10.1007/s41204-016-0001-8.

(28) Aga, K. W.; Efa, M. T.; Beyene, T. T., Effects of Sulfur Doping and Temperature on the Energy Bandgap of ZnO Nanoparticles and Their Antibacterial Activities. ACS Omega 2022, 7 (12), 10796-10803https://doi.org/10.1021/acsomega.2c00647

(29) Mourdikoudis, S.; Pallares, R. M.; Thanh, N. T. K. Characterization Techniques for

Nanoparticles: Comparison and Complementarity upon Studying Nanoparticle Properties. *Nanoscale* **2018**, *10* (27), 12871–12934. https://doi.org/10.1039/c8nr02278j.

(30) Talib, R. A.; Abdullah, M. J.; Mohammad, S. M.; Ahmed, N. M.; Allam, N. K. ZnO Nanorods/Polyaniline-Based Inorganic/Organic Heterojunctions for Enhanced Light Sensing Applications. *ECS J Solid State Sci Technol* **2016**, *5* (3), P142–P147. https://doi.org/10.1149/2.0031603jss.

(31) Malanagahalli, S.; Murera, D.; Martín, C.; Lin, H.; Wadier, N.; Dumortier, H.; Vázquez, E.; Bianco, A. Few Layer Graphene Does Not Affect Cellular Homeostasis of Mouse Macrophages. *Nanomaterials* **2020**, *10* (2). https://doi.org/10.3390/nano10020228.

(32) Tamesgen, T.; Ameya, M. A.; Sisay, G.; Yuanqi, L.; Kai, Z.; Beyene, T. T., Harnessing the power of S/N-doped NiO nanoparticles through bandgap tuning to achieve enhanced photocatalytic and antibacterial performances. Scientific Reports 2025, 15 (1), 28035, https://doi.org/10.1038/s41598-025-13151-8

(33) Shawono, B. G.; Etefa, K. T.; Muleta, G. G.; Kai, Z.; Beyene, T. T. Eco-Friendly Synthesis of Ag-Doped CuO Nanocomposites Using Solanum Tuberosum Peel Extract, Showcasing Enhanced Antimicrobial, Antioxidant, and Photocatalytic Performance. *Inorg Chem Commun* **2025**, *180* (May). https://doi.org/10.1016/j.inoche.2025.114993.

(34) Aadnan, I.; Zegaoui, O.; El Mragui, A.; Moussout, H.; Esteves da Silva, J. C. G. Structural, Optical and Photocatalytic Properties under UV-A and Visible Lights of Co–, Ni- and Cu-Doped ZnO Nanomaterials. Comparative Study. *Arab J Chem* **2024**, *17* (1), 105336. https://doi.org/10.1016/j.arabjc.2023.105336.

(35) Muhammad, A. S. PHOTOCATALYTIC DEAGRADATION OF RHODAMINE B DYE USING Mn DOPED ZnO NANOPARTICLES. *Appl J Environ Eng Sci* **2022**, *8* (4), 4–8.

(36) Lei, X.; Cao, Y.; Chen, Q.; Ao, X.; Fang, Y.; Liu, B. ZIF-8 Derived Hollow CuO/ZnO Material for Study of Enhanced Photocatalytic Performance. *Colloids Surfaces A Physicochem Eng Asp* **2019**, *568*, 1–10. https://doi.org/10.1016/j.colsurfa.2019.01.072.

(37) Pirhashemi, M.; Habibi-Yangjeh, A.; Rahim Pouran, S. Review on the Criteria Anticipated for the Fabrication of Highly Efficient ZnO-Based Visible-Light-Driven Photocatalysts. *J Ind Eng Chem* **2018**, *62*, 1–25. https://doi.org/10.1016/j.jiec.2018.01.012.

(38) Bekru, A. G.; Tufa, L. T.; Zelekew, O. A.; Goddati, M.; Lee, J.; Sabir, F. K. Green Synthesis of a CuO-ZnO Nanocomposite for Efficient Photodegradation of Methylene Blue and Reduction of 4-Nitrophenol. *ACS Omega* **2022**, *7* (35), 30908–30919. https://doi.org/10.1021/acsomega.2c02687.

(39) Renuka, L.; Anantharaju, K. S.; Vidya, Y. S.; Nagaswarupa, H. P.; Prashantha, S. C.; Nagabhushana, H. Synthesis of Sunlight Driven ZnO/CuO Nanocomposite: Characterization, Optical, Electrochemical and Photocatalytic Studies. *Mater Today Proc* **2017**, *4* (11), 11782–11790. https://doi.org/10.1016/j.matpr.2017.09.095.

(40) Babapour, H.; Jalali, H.; Mohammadi Nafchi, A. The Synergistic Effects of Zinc Oxide Nanoparticles and Fennel Essential Oil on Physicochemical, Mechanical, and Antibacterial Properties of Potato Starch Films. *Food Sci Nutr* **2021**, *9* (7), 3893–3905. https://doi.org/10.1002/fsn3.2371.

(41) Khare, S. R.; Pal, D. S.; Adhikary, D. K.; Laha, D.; Acharya, K. Applications of Nanoparticles to Enhance Shelf Life of Guava (Psidium Guajava L.) Fruits. *Int J Adv Biochem Res* **2024**, *8* (2), 653–655. https://doi.org/10.33545/26174693.2024.v8.i2h.648.

(42) Eben, S. S.; Imlay, J. A. Excess Copper Catalyzes Protein Disulfide Bond Formation in the Bacterial Periplasm but Not in the Cytoplasm. *Mol Microbiol* **2023**, *119* (4), 423–438. https://doi.org/10.1111/mmi.15032.

(43) Bisht, G.; Rayamajhi, S. ZnO Nanoparticles: A Promising Anticancer Agent. *Nanobiomedicine* **2016**, *3*. https://doi.org/10.5772/63437.

(44) Wong, F.; Stokes, J. M.; Cervantes, B.; Penkov, S.; Friedrichs, J.; Renner, L. D.; Collins, J. J. Cytoplasmic Condensation Induced by Membrane Damage Is Associated with Antibiotic Lethality. *Nat Commun* **2021**, *12* (1). https://doi.org/10.1038/s41467-021-22485-6.

Supplementary Files

This is a list of supplementary files associated with this preprint. Click to download.

- NatsanetSI081925.docx